Journal of Cleaner Production 230 (2019) 1276–1286

Contents lists available at ScienceDirect

Journal of Cleaner Production

journal homepage: www.elsevier.com/locate/jclepro

Removal of zinc based on a screw manufacturing plant wastewater by fluidized-bed homogeneous granulation process

Nutnapong Udomkitthaweewat [a, b], Jin Anotai [c], Angelo Earvin Sy Choi [d], Ming Chun Lu [a, *]

[a] Department of Environmental Resources Management, Chia Nan University of Pharmacy and Science, Tainan, 71710, Taiwan
[b] Department of Environmental Engineering, Faculty of Engineering, King Mongkut's University of Technology Thonburi, Bangkok 10140, Thailand
[c] Center of Excellence on Hazardous Substance Management, Department of Environmental Engineering, Faculty of Engineering, King Mongkut's University of Technology Thonburi, Bangkok 10140, Thailand
[d] National Research Center for Disaster-Free and Safe Ocean City, Busan 49315, Republic of Korea

ARTICLE INFO

Article history:
Received 25 October 2018
Received in revised form
2 May 2019
Accepted 17 May 2019
Available online 20 May 2019

Keywords:
Fluidized-bed homogeneous granulation process
Hydrozincite
Nucleation
Ferric ions
Chloride
Zinc crystallization

ABSTRACT

Wastewater derived from screw producing manufacturing plants contains high zinc concentrations that needs to be treated prior to its discharge. Crystallization through the fluidized-bed reactor has been an effective technology for the removal of heavy metals. In this research, the removal of zinc from a simulated wastewater was investigated by a fluidized-bed reactor. The properties of the granules were characterized by utilizing the X-ray diffraction, energy dispersive spectrometer and scanning electron microscope. A comparison of the fluidized-bed reactor setting was conducted to compare the processes of fluidized-bed homogeneous granulation and fluidized-bed granulation. Results showed that the fluidized-bed homogeneous granulation outperformed fluidized-bed granulation in terms of removal and granulation efficiencies. The essential variables for analysis include chloride concentration (0–7,000 mg/L), pH (6.9–7.5), carbonate to zinc molar ratio (1–2.5) and ferric ion concentration (0–150 mg/L) in the fluidized-bed homogeneous granulation process. The results indicated that the ideal conditions for hydrozincite granulation were at a carbonate to zinc molar ratio of 1.2 and pH 7.2. The elemental composition analysis of the hydrozincite revealed zinc contents of the following: (1) absence of chloride (63.71 wt% zinc), (2) presence of chloride (63.08 wt% zinc) and (3) presence of ferric ions (52.62 wt% zinc). The inclusion of chloride and ferric ions in the system interfered with zinc precipitation and granulation. Furthermore, the hydrozincite granule predominantly reached a diameter of 149 μm (with chloride) and 42 μm (with ferric ions).

1. Introduction

A rapid rise in global population and industrialization has caused an unprecedented decline in fresh water resources and an upsurge in wastewater discharges. Various soluble heavy metals are typically present in the effluents coming from manufacturing or domestic sources that perceives long-term environmental concerns. Manufacturing processes such as in screw production plants emit hazardous complex mixtures of organic matters and heavy metals in their effluent that would lead to the disruption of water quality if left untreated (Boonrattanakij et al., 2018). Typically, an untreated wastewater from a screw producing plant generates a high concentration of zinc (Zn) (Boonrattanakij et al., 2018). The World Health Organization has set a threshold value of 3 mg/L Zn for drinking water (WHO, 2003). At trace amounts, Zn is an essential element that functions as an enzyme activator in animals and humans (Quiton et al., 2018). However, Zn at excessive concentrations can cause detrimental impacts towards aquatic living species, humans and plants. A Zn concentration of 2 mg/L can adversely affect the oxygen level in the blood of fish (Porea et al., 2000). At concentrations beyond the permissible level, Zn can lead to a malfunction of various systems in the human body (Bhattacharya et al., 2006). Zn is also poisonous to plants at high concentrations and can be damaging in soils because of its high mobility (Freitas et al., 2017). Thus, the proper treatment of the wastewater requires to be appropriately handled prior to its disposal.

The removal of Zn from various waste sources has been

---

* Corresponding author. Tel.: +886 6 266 0489; fax: +886 6 266 3411.
E-mail address: mmclu@mail.cnu.edu.tw (M.C. Lu).

https://doi.org/10.1016/j.jclepro.2019.05.192

considered by utilizing numerous methods as follows: (1) electrodialysis enhanced with complex formation method in a simulated electroplating industry waste (Babilas and Dydo, 2018), (2) supergravity separation using a centrifugal apparatus in an industrial galvanizing dross (Wang et al., 2018), (3) leaching by ultrasound technique in a zinc oxide flue dust (Zheng et al., 2015), (4) bioleaching by *Acidithiobacillus thiooxidans* in Zn metallurgical leach residues (Sethurajan et al., 2017) and (5) adsorption using active silicon adsorbent in leaching residue from lead-zinc tailings (Lei et al., 2018) and utilizing the adsorbent of chitosan-coated montmorillonite beads in a synthetic wastewater (Tsai et al., 2016). Nevertheless, the aforementioned processes have not focused on the prospect of Zn recoverability in its system. Chemical precipitation is the most commonly used method that produces precipitant products in the form of sulfides and hydroxides (Peng et al., 2014). However, the accumulation of sludge translates to an increase in cost in terms of the dewatering requirement that works as a disadvantage in this process (Lee and Lee, 2005). Other drawbacks of the precipitation method include the need of a larger space for treatment and the potential recoverability of the target metal is infeasible (De Luna et al., 2015; Guevara et al., 2017).

The fluidized-bed reactor (FBR) typically utilizes a granulation technique that employs fluidized seeds to stimulate crystallization that therefore addresses the need of a lesser space for disposal than does in the precipitation method (Järvinen et al., 2015; Shih et al., 2017). FBR also presents several advantages against the conventional precipitation method such as utilizing fewer chemicals and recovering the granules or crystallized particles (Caddarao et al., 2018). In recent years, a commonly used FBR setup for crystallization is the fluidized-bed granulation (FBG) process. This is due to its associated lower operating cost and high recovery efficiency of heavy metals in waste streams. Past studies of the FBG process have treated inorganic pollutants such as copper (Chung et al., 2015), iron (Anotai et al., 2018), lead (De Luna et al., 2015), sulfate (De Luna et al., 2017) and phosphate (Su et al., 2014). Currently, there are limited studies in previous researches that particularly focuses on the removal of Zn in relation to crystallization in the FBG setup.

The main disadvantage in the FBG process is the dependency on seeding materials such as silica (SiO_2) to support appropriate crystal growth (Caddarao et al., 2018). This process promotes a heterogeneous nucleation in the system that produces a final product made out of crystals covered onto the surface of the seeding component. This adversely influences the recyclability of the recovered crystals because of the impurity in its core (Chen et al., 2015). To solve this drawback, the fluidized-bed homogeneous granulation (FBHG) process has recently been put to attention as an alternative technique in the FBG process. The final product in the FBHG does not have a seeding requirement to purify the granule crystals due to undergoing homogeneous crystallization (Salcedo et al., 2016). The process for supersaturation functions at mild conditions where the agglomerated fine nuclei at moderate amounts forms adequate active sites to stimulate high-purity granules from a homogeneous crystal growth (Caddarao et al., 2018). Specifically, the influent metal salts in the FBHG process are able to gather sufficient active surfaces that produce homogeneous granules (Salcedo et al., 2016). Particle growth and nucleation steps occur afterwards. This would then generate particles having a larger mass with high-purity. The FBR in the FBHG process comprise of water interactions that are similarly present in traditional precipitation processes. However, the granulation mechanism and nuclei development in the FBHG process can be estimated through the hydraulic conditions in the metastable region (Chen et al., 2015). This would lead to the formation of dense granules rather than soft sludge. Furthermore, the FBHG process in previous literature has investigated the treatment of aluminum (Vilando et al., 2019), oxalate (Guevara et al., 2017), phosphate (Caddarao et al., 2018; Su et al., 2014), lead (Chen et al., 2015) and nickel (Ballesteros et al., 2016; Salcedo et al., 2016). To date, no studies have yet examined the removal of Zn under the FBHG process.

Thus, the novelty in this research work focuses on the removal of Zn investigated primarily in the FBHG process. Furthermore, a simulated wastewater based on a screw producing manufacturing plant was utilized in the experimental runs. The resulting granules were characterized subjected to various conditions over FBHG to assess the crystalline composition, elemental composition and surface morphology. A comparative assessment of the FBG and FBHG processes were examined to determine its effectivity in crystallization. The effect of chloride concentration, pH, $[CO_3^{2-}]$:$[Zn^{2+}]$ molar ratio and ferric ion concentration were systematically studied to evaluate the Zn removal efficiency, granulation efficiency and granulation size in the FBHG.

2. Experimental

2.1. Materials

Zinc sulfate heptahydrate ($ZnSO_4 \cdot 7H_2O$: 99.5% purity), sodium carbonate (Na_2CO_3: 99.0% purity), nitric acid (HNO_3: 69% purity) and sulfuric acid (H_2SO_4: 96% purity) were procured from Panreac, Spain. Sodium hydroxide (NaOH: 98% purity), sodium chloride (NaCl: 99.5% purity) and ferric chloride ($FeCl_3$: 99.0% purity) were purchased from Shimakyu Chemical, Taiwan. Screw wastewater was obtained from a screw manufacturing industry in Kaohsiung, Taiwan. All chemicals used were reagent grade and without further purification treatment.

2.2. Instrumentation

The Zn concentrations were analyzed using an atomic absorption spectrophotometer (AAS: PerkinElmer, AAnalyst 200). The X-ray diffraction (XRD: Bruker D8, USA) was utilized to determine the crystalline composition of the FBHG products. The samples were placed in a holder that were subjected to the XRD machine with a copper target ($\lambda = 15.406$ nm) using a germanium monochromator. The data for the XRD analysis was collected in the diffraction angle ranging from 0 to 70°. The diffraction patterns were manually evaluated utilizing the powder diffraction standards. The elemental composition of the crystallized granules is determined through an energy dispersive spectrometer (EDS: FEI Genesis XM 4i, Austria). The surface morphology of the generated crystals from the FBHG process was determined with the use of a scanning electron microscope (SEM, FEI Quanta 200 Environmental Scanning Electron Microscope, Austria). The SEM under a vacuum employs a tungsten filament that operated at an accelerating voltage of 20 kV. A thin layer of gold was coated with the crystalline samples using a sputter coater.

2.3. Fluidized-bed reactor set-up

A 0.55 L glass-cylinder reactor comprising of an inlet, outlet, and a recirculation pump as illustrated in Fig. 1 was used as the FBR. A simulated wastewater and sodium carbonate solution were continuously fed into the FBR by the peristaltic pumps. The reactor was filled with 0.5 cm diameter glass beads to the height of 4.0 cm. Furthermore, the FBR was operated in a continuous process. The pH of the solution was regulated at a specified value by the addition of either H_2SO_4 or NaOH whenever necessary in the synthetic wastewater. The expansion of the fluidized bed was controlled by a recirculation pump. In the FBR, an appropriate amount of the sample was taken for the analysis at a predetermined time. Soluble

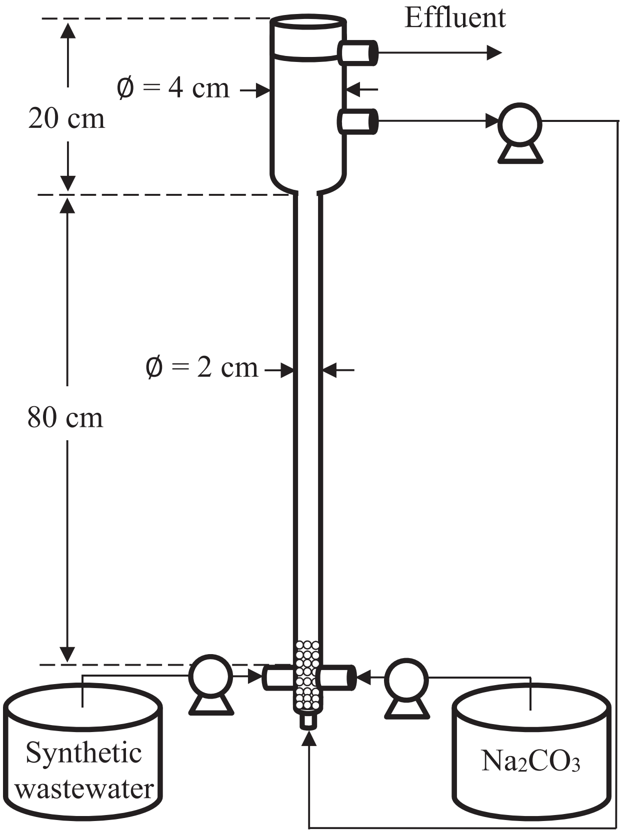

Fig. 1. Fluidized-bed reactor.

Zn concentration was determined utilizing the AAS. For total Zn measurement, the sample was digested with HNO_3. On the other hand, the simulated wastewater and the carbonate precipitant solution were pumped into the reactor at equal flow rates at 25 mL/min was initially set for the actual fluidization of the FBR. The recirculation rate was started at 30 mL/min and increased up to 300 mL/min depending on the fluidization state and the granule growth characteristics inside the reactor.

2.4. Experimental procedures

All runs lasted for 7 days without interruption. The detailed chemical composition of the synthetic and real wastewater are listed in Table 1. Furthermore, the influent Zn concentration was kept constant at 500 mg/L in all the experimental runs to simulate the wastewater coming from a screw factory in Taiwan. The total removal of Zn can be attained after filtration of the treated effluent from the FBR that can be measured in Eq. (1). All the formed granules refer to the Zn that were removed from the simulated wastewater. Moreover, the granulation efficiency pertains to the Zn granules that formed during the fluidization process as calculated in Eq. (2).

Table 1
Chemical composition of the synthetic and real wastewater.

Chemical composition	Synthetic wastewater	Real wastewater
Zinc concentration (mg/L)	500	106 to 499
Chloride concentration (mg/L)	0 to 7,000	4,020 to 5,020
$[CO_3^{2-}]:[Zn^{2+}]$ molar ratio	1.0 to 2.5	
Ferric ion concentration (mg/L)	0 to 150	

$$\mathrm{ZnRemoval}(\%) = \frac{C_0 - C_D}{C_0} \times 100 \tag{1}$$

$$\mathrm{Granulation}(\%) = \frac{C_0 - C_T}{C_0} \times 100 \tag{2}$$

where C_0 is the initial Zn concentration in the simulated wastewater, C_T is the total concentration of Zn in the effluent, and C_D is the concentration of dissolved Zn after the fluidized-bed treatment.

2.4.1. Evaluation of FBHG and FBG

The experimental conditions were performed at a constant pH (7.2), $[CO_3^{2-}]:[Zn^{2+}]$ molar ratio (1.2), chloride concentration (0 mg/L and 5,000 mg/L) and seed bed (0 g, 50 g (hydrozincite) and 50 g (silica sand)) to evaluate the efficiency of Zn removal through the granulation of zinc carbonate in the FBG and FBHG process reactors. The Zn removal and granulation were thus utilized to evaluate the efficacy in FBR.

2.4.2. Chloride variation

The effect of varying the chloride concentration (0 mg/L, 2,000 mg/L, 3,000 mg/L, 5,000 mg/L and 7,000 mg/L) on the granulation and removal efficiency of the FBHG process. These parameters were selected to simulate the wastewater that contains high chloride content. The $[CO_3^{2-}]:[Zn^{2+}]$ molar ratio of 1.2 and pH of 7.2 were kept constant to determine the impact of chloride on the precipitation of zinc carbonate in a simulated wastewater.

2.4.3. pH variation

Various pH levels of 6.9, 7.1, 7.2, 7.3 and 7.5 were used to study the effect of the pH solution in the aspect of Zn removal in a FBHG process. A $[CO_3^{2-}]:[Zn^{2+}]$ molar ratio of 1.2 and chloride concentrations of 0 mg/L and 5,000 mg/L were set as its parameters to identify the influence of pH for Zn granulation and removal.

2.4.4. $[CO_3^{2-}]:[Zn^{2+}]$ molar ratio variation

In the FBHG process, the $[CO_3^{2-}]:[Zn^{2+}]$ molar ratios were set at 1.0, 1.2, 1.5, 2.0 and 2.5 to determine a suitable ratio for Zn removal. The pH (7.2) and chloride concentration (5,000 mg/L) were maintained constant to appropriately control and monitor the effect of $[CO_3^{2-}]:[Zn^{2+}]$ molar ratio towards the precipitation of Zn in the simulated wastewater.

2.4.5. Ferric ion variation

In actual wastewater from screw manufacturing plants, the cleaning steps of the manufacturing process produce ferric ion contents in its wastewater. In order to determine its influence towards the precipitation of Zn, various ferric ion concentrations (0 mg/L, 5 mg/L, 10 mg/L, 30 mg/L, 50 mg/L, 100 mg/L and 150 mg/L) independent of additional chloride (0 mg/L) were added to simulate a wastewater based from screw manufacturing plants. Moreover, the other parameters were controlled at a $[CO_3^{2-}]:[Zn^{2+}]$ molar ratio of 1.2 and pH 7.2 to assess the impact of ferric ions on the precipitation of zinc carbonate and understand the crystallization behavior between Zn^{2+} and Fe^{3+}.

3. Results and discussion

3.1. Crystalline phase characterization

Fig. 2 (a) – (d) illustrates the XRD diffractograms of the crystalline samples at various conditions in the FBHG process. The Joint Committee on Powder Diffraction Standards (JCPDS) No. 19–1458 for hydrozincite ($Zn(CO_3)_2(OH)_6$) is shown in Fig. 2 (a). The result in

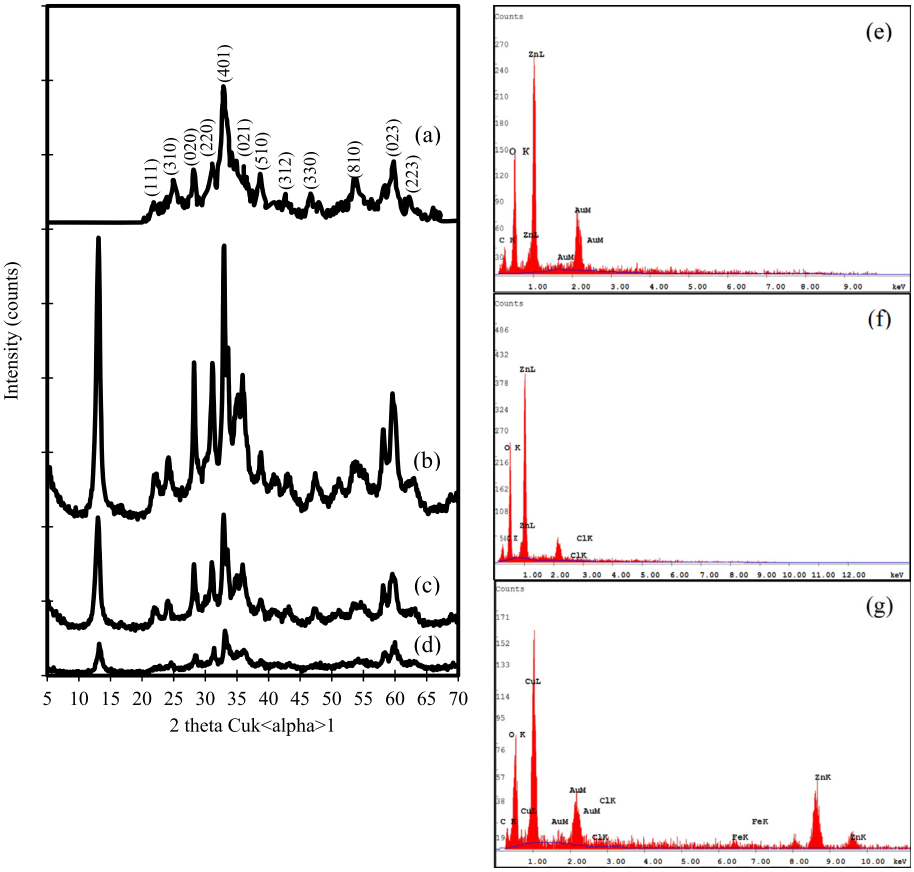

Fig. 2. XRD patterns in various settings: (a) $Zn_5(CO_3)_2(OH)_6$ (JCPDS 19–1458), (b) absence of chloride, (c) with 5,000 mg/L Cl^- and (d) with 50 mg/L Fe^{3+} and EDS analysis spectrums results in different conditions: (e) without electrolyte, (f) with chloride and (g) with ferric chloride.

the XRD pattern of Fig. 2 (b) showed that the granule formed in the absence of chloride and ferric ions mainly constitutes $Zn_5(CO_3)_2(OH)_6$ due to the parallel peaks displayed in JCPDS No. 19–1458 (Cheng and Poduska, 2013). Moreover, the broad diffraction peaks implied that the presence of amorphous zinc compounds is co-existing with the granule sample. In the presence of chloride (Fig. 2 (c)) and ferric ions (Fig. 2 (d)), both its XRD results showed peaks that confirms the existence of hydrozincite. However, the peaks were considerably lower due to the development of chloride interferences and ferric ion inhibitions. Therefore, it can be established that chloride and ferric ions had a substantial impact towards the precipitation of hydrozincite.

3.2. Elemental distribution

The EDS spectrums of the samples before and after chloride addition are shown in Fig. 2 (e) and (f), while Fig. 2 (g) pertains to the EDS spectrum of the sample containing ferric ions in the FBHG process. Results indicate that the elements constituting the products are essentially Zn, carbon and oxygen. These are the main components of hydrozincite. On the other hand, the presence of gold (Au) was detected due to sputtering. Therefore, Au would be disregarded in the analysis. The absence of chloride peak validates the result of the chloride being nonexistent in Fig. 2 (e). Furthermore, Zn salts were formed in the FBR. The effects of the removal or conversion were thus primarily attributed to the interference of the direct interactions between Zn and carbonate ions.

Table 2 lists the elemental composition of the granules obtained from the EDS analysis. It was found that the recovered hydrozincite based on Zn composition in the granules obtained a purity of 63.71 wt% (absence of chloride), 63.08 wt% (presence of chloride) and 52.62 wt% (presence of ferric ions). The results indicate that the crystal products from the FBHG process (with or without the presence of chloride) were of high purity. This may potentially be further processed for its reuse in screw manufacturing processes or other suitable applications in various industries.

Table 2
EDS results: Elemental composition analysis.

Experiment	Unit	Element					
		Carbon	Oxygen	Zinc	Chloride	Iron	Total
without electrolyte	*Wt %	15.36	20.93	63.71	–	–	100
	**At %	35.90	36.73	27.37	–	–	100
with chloride	*Wt %	12.50	23.72	63.08	0.69	–	100
	**At %	29.67	42.26	27.51	0.56	–	100
with ferric ions	*Wt %	14.93	29.22	52.62	0.76	2.46	100
	**At %	31.55	46.35	0.55	1.12	20.43	100

*Weight percent.
**Atomic percent.

3.3. Surface morphology

The morphologies and structure of the granules were analyzed using SEM in the FBHG process. Fig. S1 illustrates the image of granules obtained from the experimental runs. The hydrozincite depicted in the micrographs consist of a morphological characteristic with botryoidal masses similarly reported in the study of Ngwenya et al. (2014). A longer time was necessary for the core nuclei to be generated through the mechanisms of agglomeration and grain growth. This was because of the system that has undergone a homogeneous crystallization process. In the absence of chloride (Figs. S1 (a) and (b)), results revealed that the agglomerates consist of granule structures that sticks together. This specifically appeared to have a smooth and stable rounded surface. However, the individual application of chloride (Figs. S1 (c) and (d)) and ferric ions (Figs. S1 (e) and (f)) have made their respective structure smaller. This is attributed to the interference of chloride and inhibition of ferric ions towards the formation of hydrozincite. Furthermore, the micrograph for the inclusion of chloride in Figs. S1 (c) and (d) were formed due to the collision of the anions that did not result from a bond formation. The chloride ions may have specifically collided with zinc ions. Since $ZnCl_2$ is readily soluble in aqueous solution, this would dissolve right after the reaction and caused the ions to fail to attain any chemical bonds. Based on the result of the SEM analysis, this confirms the mechanism of nuclei formation, fine nuclei aggregation and crystal growth in the FBHG process.

3.4. Comparison of FBHG and FBG

A comparative assessment of FBHG process (without seeds and using hydrozincite) and FBG process (using silica sand as seeds) was done in terms of its granulation method before and after the addition of chloride. Fig. 3 (a) shows the comparative results of Zn removal and granulation efficiencies between FBHG and FBG at 500 mg/L Zn and pH 7.2. In the absence of chloride, the removal and granulation efficiencies of FBHG (without seeds) were 97.56%, and 93.39%. Furthermore, the use of hydrozincite seeding in FBHG lead to efficiencies of 91.15% (removal) and 88.72% (granulation). These results indicate the superior performance of FBHG over FBG (using silica sand as the fluidized material) that only yielded 83.18% and 80.90% for the removal and granulation efficiencies. On the other hand, the presence of 5,000 mg/L chloride significantly dropped the removal and granulation efficiencies of FBHG (without seeds) to 89.29% and 86.67%, and FBHG (hydrozincite seeding) to 83.17% and 82.97%. For FBG, the efficiencies also dropped the efficiencies to 81.97% for removal and 80.10% for granulation. As a result, FBHG still outperformed the FBG in the presence of chloride in the aspect of Zn removal and granulation. Based on Fig. 3 (b) and (c), high Zn removal were already achieved at 6 h. For the FBG process using silica seed at the reaction time of 6 h–7 days, the remaining Zn concentration was roughly at (87 ± 4) mg/L (without chloride) and (90 ± 3) mg/L (with chloride). On the other hand, the FBHG process without seed application resulted to (19 ± 6) mg/L Zn (without chloride) and (56 ± 10) mg/L (with chloride). Both the FBG and FBHG processes have not met the maximum drinking water limit of 3 mg/L Zn set by the World Health Organization (WHO, 2003). However, the FBHG process gave promising results against the FBG process in retaining a lower Zn concentration notable for further investigation.

The homogeneous nucleation in a FBHG led to the formation of the enormous amount of tiny nuclei dispersing throughout the

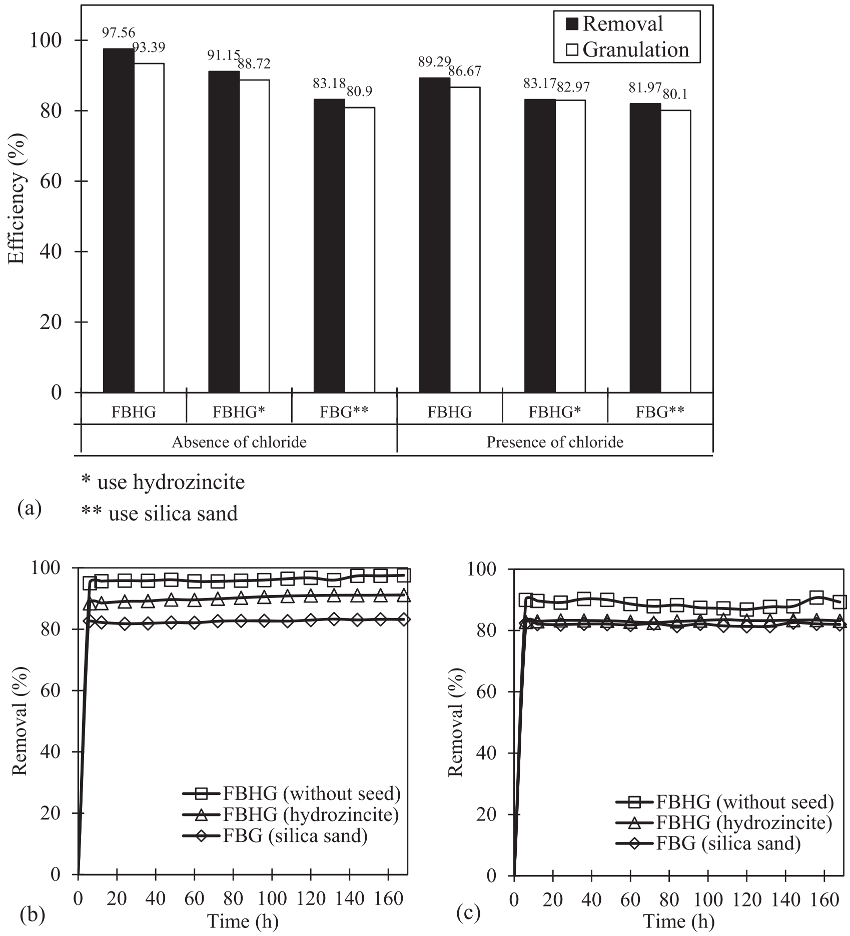

Fig. 3. (a) Comparison of FBHG and FBG on the efficiencies of Zn (500 mg/L) removal and granulation at pH 7.2, percentage of Zn removal in the (b) absence and (c) presence of 5000 mg/L chloride.

entire reactor. Due to a rapid expansion of the reactor at the upper part, the upflow velocity dropped greatly which allowed the fine colloids to undergo coagulation and flocculation. These eventually became larger and denser aggregates. The heavy particles then sank to the bottom part of the reactor due to a higher settling velocity that became fluidized by the recirculation flow. At this phase, the grain growth in the FBHG by a heterogeneous nucleation and granulation resembles that of the FBG. The FBHG process during heterogeneous nucleation resulted in a support in the form of a homogeneous complex that showed a common ion effect (Chen et al., 2015). This in turn reduces the solubility of the zinc carbonate within the solid–liquid interface. Moreover, the sands utilized in the FBG process exerted a physical force towards the particle collision greater than the aggregates in the FBHG. This promoted the attrition and layering of the coated hydrozincite. Henceforth, the FBHG yielded larger primary particles than the FBG (Chen et al., 2015). Moreover, the study of Chen et al. (2015) for the removal of lead in FBR using sodium carbonate as the precipitant found that, without adding the seed materials, the FBHG acquired purer lead carbonate than the FBG process. This proves to show the consistency of the results found in this study. Therefore, the primary focus of this research is towards the utilization of FBHG process to determine the feasibility of Zn removal and granulation in a model wastewater based on a screw manufacturing plant.

3.5. *Effect of chloride*

Industrial effluent produced from screw manufacturing plants typically contains a high chloride concentration. This is due to the conventional application of chloride in the rapid mixing tank as its coagulant and precipitant prior to entering the flocculation tank (Boonrattanakij et al., 2018). Hence, the interaction of chloride can affect the precipitation of Zn in its wastewater. The experiment was conducted to determine the impact of chloride on the precipitation of hydrozincite.

In this section, chloride was selected as anionic species. The calculated values are given in Table 3. The ionic strength is a measure of the concentration of ions in the solution. The total electrolyte concentration in the solution affects important properties of the dissociation or the solubility of different salts. One of the main characteristics of a solution with dissolved ions is its ionic strength. The effect of the addition of ionic strength (through the addition of ions), the ionic strength (μ) of the solution and the ionic activities were calculated using the extended Debye-Huckel (applicable at $\mu < 0.1$ mol/L) and Davies (applicable at $\mu < 0.5$ mol/L) equations given in Eqs. (4) and (5) (Benjamin, 2001).

$$\mu = 0.5c_i z_i^2 \tag{3}$$

$$-\log\gamma_i = \frac{Az_i^2\sqrt{\mu}}{1+B\propto\sqrt{\mu}} \tag{4}$$

$$-\log\gamma_i = Az_i^2\left(\frac{\sqrt{\mu}}{1+\sqrt{\mu}} - 0.2\mu\right) \tag{5}$$

where μ refers to ionic strength (mol/L), z_i, c_i and γ_i are the charge, concentration and activity coefficient of the ion species, α denotes the ion size (Å), while A and B are temperature-dependent parameters of 0.509 $(\text{mol/L})^{-1}$ and 0.328 Å^{-1} $(\text{mol/L})^{-1}$.

Furthermore, the effect of chloride on Zn removal was investigated by varying the chloride concentrations from 2,000 mg/L to 7,000 mg/L at the conditions of 500 mg/L Zn, $[CO_3^{2-}]:[Zn^{2+}]$ molar ratio of 1.2 and pH 7.2. It is notable to mention that the aqueous solubility of zinc chloride is considerably higher than that of zinc carbonate and hydrozincite (Clever et al., 1992); henceforth, the chloride range used in this study would essentially not have any substantial impact on hydrozincite, $Zn_5(CO_3)_2(OH)_6$, precipitation as presented in Eqs. (6) and (7) (Fischer and Peters, 1970). The removal and granulation efficiencies were plotted versus the chloride concentration as illustrated in Fig. 4 (a). In the absence of chloride, the removal and granulation efficiencies were 97.56% and 93.39%. This implies that 4.17% of the Zn precipitates were suspended in the solution. In contrast, the removal and granulation efficiencies trended to be lower in the presence of chloride that dropped by 2.62%–7.98%.

$$Zn_5(CO_3)_2(OH)_6 \rightarrow 5Zn^{2+} + 2CO_3^{2-} + 6OH^- \; K_{sp} = 2\times10^{-9} \tag{6}$$

$$ZnCl_2 \rightarrow Zn^{2+} + 2Cl^- \; K_{sp} = 31.7 \tag{7}$$

Various ions were present in the simulated wastewater (Zn^{2+}, SO_4^{2-}, Na^+ and Cl^-) and the precipitant solution (Na^+ and CO_3^{2-}). The spectator ions in the system were SO_4^{2-} because of zinc sulfate, Na^+ due to sodium chloride and sodium carbonate, and the OH^- in the sodium hydroxide used to control the pH of the precipitant. Moreover, the addition of chloride ions at varying concentrations (2,000 mg/L to 7,000 mg/L) lead to higher ionic strength from 0.0680 (without chloride) to 0.1397 to 0.3189 as listed in Table 3. This resulted towards a decrease in terms of the activities associated with OH^-, Zn^{2+} and CO_3^{2-}. Thus, the addition of chloride ions reduced the activities of all ions involving the $Zn_5(CO_3)_2(OH)_6$ precipitation which has led to lower removal and granulation efficiencies.

In addition, chloride ion also affected the granulation size as depicted in Fig. 4 (b). It was found that, in the absence of chloride, 18.71% of the granules had a diameter of 1.0 mm or larger. However, the diameter of the granules decreased by 9.50% (2,000 mg/L),

Table 3
Ionic strength of ion species for 500 mg/L Zn^{2+} and molar ratio $[CO_3^{2-}:Zn^{2+}]$ of 1.2

Experiment	Ionic Strength[a] (M)		Ion Species		
			Zn^{2+}	CO_3^{2-}	Cl^-
Control	0.0680	γ_i	0.4458	0.4247	–
		Activity (mg/L)	222.90	233.87	–
with 2,000 mg/L Cl^-	0.1397	γ_i	0.3184	0.3184	0.7512
		Activity (mg/L)	159.19	175.32	1,502.34
with 3,000 mg/L Cl^-	0.1755	γ_i	0.2952	0.2952	0.7372
		Activity (mg/L)	147.67	162.63	2,211.58
with 5,000 mg/L Cl^-	0.2472	γ_i	0.2658	0.2658	0.7180
		Activity (mg/L)	132.89	146.35	3,590.06
with 7,000 mg/L Cl^-	0.3189	γ_i	0.2483	0.2483	0.7059
		Activity (mg/L)	124.17	136.75	4,941.52

[a] Including with Na^+ and SO_4^{2-} in reactor.

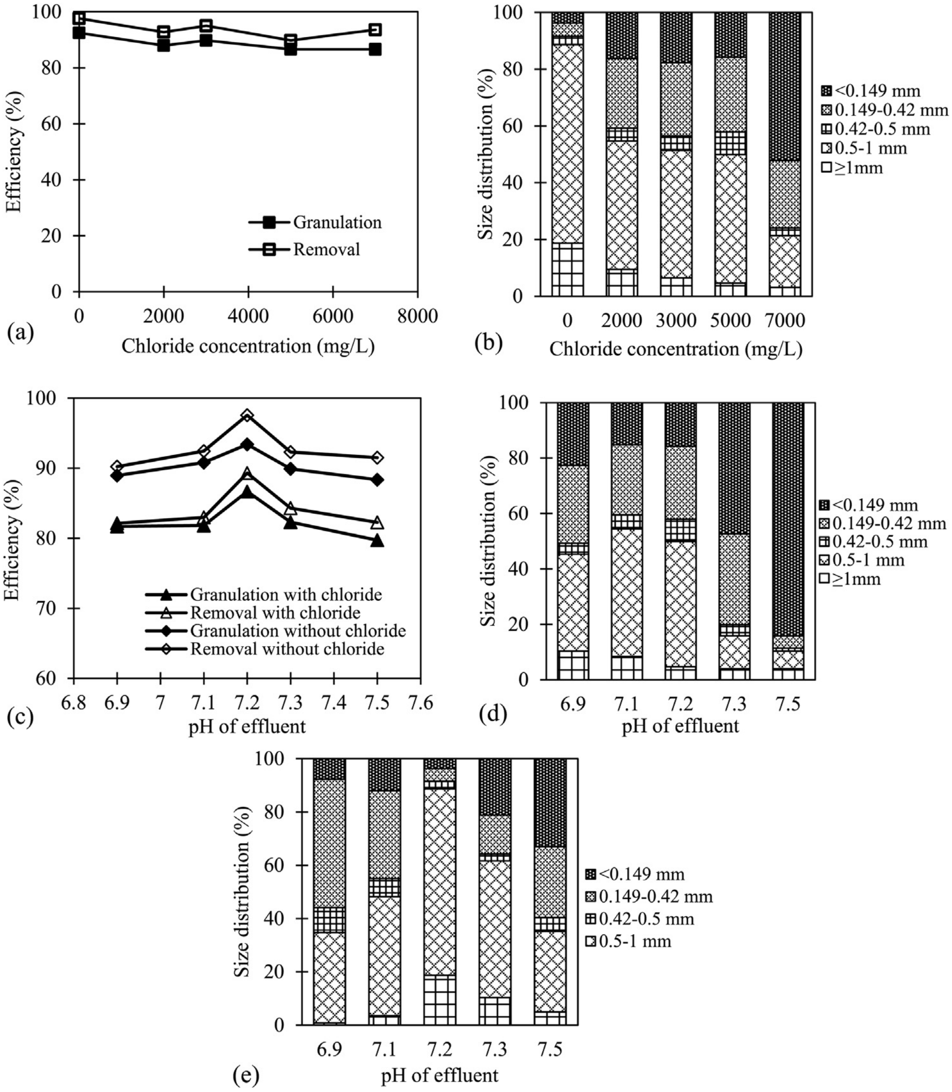

Fig. 4. Effect of chloride (a) on the removal and granulation efficiencies and (b) granules size distribution; effect of effluent pH (c) on the removal and granulation efficiencies and the granule size distribution (d) with and (e) without 5,000 mg/L Cl⁻

6.46% (3,000 mg/L), 4.68% (5,000 mg/L) and 3.10% (7,000 mg/L). This clearly indicates that chloride interfered with the granulation process.

3.6. *Influence of pH*

In Fig. 4 (c) to (e), the pH of the solution was varied from 6.9 to 7.5 with and without the addition of 5,000 mg/L chloride. The presence of chloride is essential in order to simulate the chloride concentration present in real wastewater from screw manufacturing plants. Fig. 4 (c) shows the highest removal percentage was obtained at pH 7.2 for both Zn removal (89.29%) and granulation (86.67%) efficiencies. Increasing the pH from 6.9 to 7.1 was able to promote Zn removal (82.13%–82.97%) and granulation (81.67%–81.81%) efficiencies. This is associated with the lack of supersaturation condition necessary for an effective nucleation and crystallization of zinc carbonate and zinc hydroxyl carbonate at pH 6.9 and 7.1. On the other hand, further increasing the pH to 7.3 and 7.5 resulted in the decrease of efficiencies from 84.30% to 82.29% (Zn removal) and 82.27%–79.72% (granulation). Higher alkalinity levels can enhance the formation of zinc-hydroxo complexes which might interfere with the precipitation of Zn (Forslund et al., 2014). In the absence of chloride under the same conditions, the highest removal percentage was also obtained at pH 7.2 of 97.56% for Zn removal and 93.39% for granulation. Furthermore, the efficiencies increased by 7.21%–10.23% for Zn removal and 7.19%–9.89% for granulation in the absence of chloride as compared to the simulated wastewater with 5,000 mg/L chloride.

The amphoteric tendencies of $Zn(OH)_2$ caused a dissolution of the Zn ions that produced a finer particle size. This resulted in a steep decrease in the removal and conversion efficiencies from pH 7.3 to 7.5. A further increment in the pH increases the supersaturation together with the granulation and precipitation rate that decreases the removal efficiency. A sudden decrease in granulation efficiency is attributed to the presence of impurities in the simulated wastewater sample that may also result in a decrease in the removal efficiency due to the breakage of granules (attrition) and a competing secondary nuclei formation (Rahaman and Mavinic, 2009). Similar results were observed in Zn removal with and without the presence of chloride as discussed in the previous section. NaOH was utilized for pH adjustment throughout the variation in the experimental setup that dissolved some of the precipitated

$Zn(OH)_2$. The higher the required precipitant pH, the more NaOH needed to be added to the solution for adjustment. This resulted to more $Zn(OH)_2$ being re-dissolved in the reactor which produces fines that were carried to the effluent through the upflow velocity. The relatively small quantity of re-dissolved $Zn(OH)_2$ is significantly enough to reduce the efficiencies by 6%. This is an essential factor that caused a notable decrease in the removal and granulation efficiencies from pH 7.2 to 7.5.

Furthermore, pH also had a substantial impact on the size of the granule. The highest percentage of the diameter size greater than 1.0 mm was 10.39% at pH 6.9 as depicted in Fig. 4 (d). Higher pH values sequentially decreased the percentages of the diameter size greater than 1.0 mm to 8.43% (pH 7.1), 4.68% (pH 7.2), 3.94% (pH 7.3) and 3.92 (pH 7.5). Conversely, the absence of chloride exhibited the highest percentage of the diameter size greater than 1.0 mm formed by 18.71% at pH 7.2 as illustrated in Fig. 4 (e). This proves to show the interference of chloride towards the granulation process that decreased the size of the granule to finer particle sizes. Moreover, in the presence of chloride, the highest percentage of the diameter size greater than 1.0 mm occurred at pH 6.9. This was shifted against the system in the absence of chloride at pH 7.2.

3.7. *Effect of [CO_3^{2-}]:[Zn^{2+}] molar ratio*

At [CO_3^{2-}]:[Zn^{2+}] molar ratio of 1.0, the lowest removal and granulation efficiencies were obtained. This is predominantly due to the absence of excess carbonate ions in the system that is responsible to produce $Zn_5(CO_3)_2(OH)_6$ and $ZnCO_3$ as shown in Eqs. (8) and (9). Although the number of moles of the precipitant is equal to that of Zn that satisfies the stoichiometric requirement for the reaction, the imperfect mixing of the fluid solutions in the system allowed Zn ions to remain unreacted towards the carbonate ions. Thus, ensued the Zn ions to be carried off with the effluent.

As shown in Fig. 5 (a), the highest efficiencies on the removal and granulation were obtained at the molar ratio of 1.2. As the molar ratio of carbonate to Zn increased from 1.0 to 1.2, the efficiencies increased from 80.27% to 89.29% (Zn removal) and 79.78%–86.67% (granulation). Higher molar ratios from 1.5 to 2.5 resulted in the decrease of both removal and granulation efficiencies. When the [CO_3^{2-}]:[Zn^{2+}] molar ratio is relatively high, too much CO_3^{2-} ions present in the system would accelerate the reactions in Eq. (8) – (10).

$$5Zn^{2+} + 2CO_3^{2-} + 6OH^- \rightarrow Zn_5(CO_3)_2(OH)_6 \tag{8}$$

$$Zn^{2+} + CO_3^{2-} \rightarrow ZnCO_3 \tag{9}$$

$$Zn^{2+} + 2OH^- \rightarrow Zn(OH)_2 \tag{10}$$

This in turn promotes a discrete precipitation that resulted in the formation of fines (Zhou et al., 1999). In the FBHG process, although the discrete precipitates at the bottom of the reactor are necessary for a homogeneous nucleation at the beginning of the experimental run, it should still be appropriately monitored later on to avoid the production of fine particles.

In addition, it was observed that the granules became larger as the [CO_3^{2-}]:[Zn^{2+}] molar ratio increased. A higher molar ratio resulted in the attrition of large granules. Therefore, this formed finer solids that reduced the Zn removal efficiency as depicted in Fig. 5 (b).

3.8. *Effect of ferric ions*

In an actual setting, the wastewater in screw manufacturing typically contains ferric ions as a result from the conventional methods of material and equipment washing (Boonrattanakij et al., 2018). In large quantities of inorganic chloride ions, the synergistic effect towards the ferric ions can form complexes and insoluble salts (Benjamin, 2015; Connick et al., 1956). However, the chloride component resulted from the EDS analysis in Table 2 showed only a minimal chloride content (1.12 at%) as opposed to iron (20.42 at%). Therefore, the ferric chloride used in this study is mainly tested to appropriately simulate the wastewater based on the variation of the ferric ion concentration from 5 mg/L to 150 mg/L. All the experimental runs are tested at 500 mg/L Zn concentration, [CO_3^{2-}]:[Zn^{2+}] molar ratio of 1.2 and pH 7.2. Initially, the resulting preparation for the Fe^{3+} and Zn^{2+} solution poured in the simulated wastewater tank was at pH 3.0. It was found that when ferric ion concentration was more than 30 mg/L, some components of Fe^{3+} were precipitated in the synthetic wastewater tank. This implies that, at pH 3.0, Fe^{3+} has a slightly lower solubility at 30 mg/L that leads to an oversaturation and precipitation in the form of $Fe(OH)_3$ based on the reaction of Eq. (11).

$$Fe^{3+} + 3OH^- \rightarrow Fe(OH)_3 \tag{11}$$

The results for the variation of ferric ions are presented in Fig. 6 (a). The granules obtained before the addition of ferric ions was colored white as shown in Fig. 6 (b). Upon the addition of ferric chloride, the resulting granules turned to orange in color due to the product of iron oxide in the system (Fig. S2).

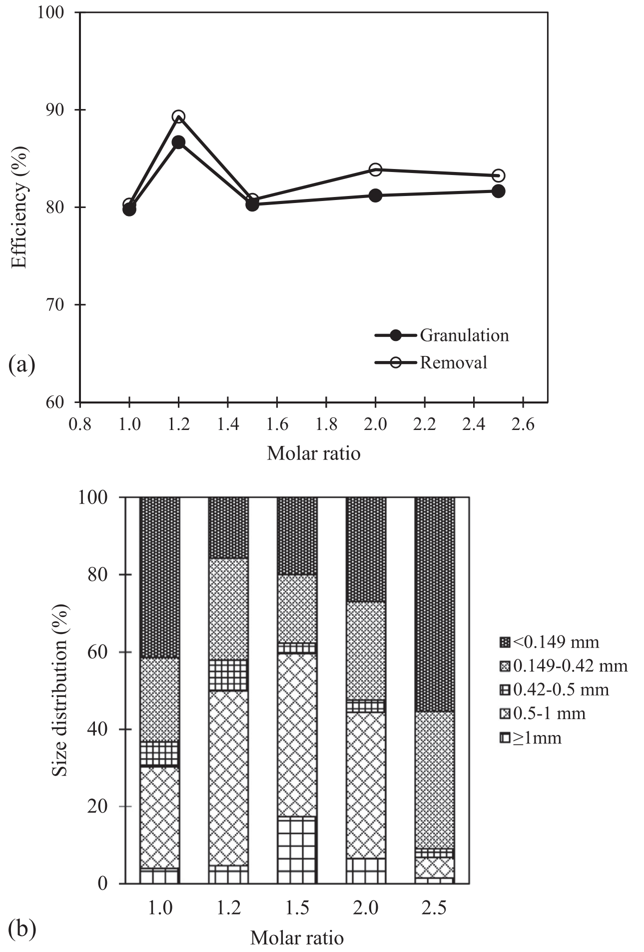

Fig. 5. Effect of molar ratio (a) on the removal and granulation efficiencies and (b) granules size distribution.

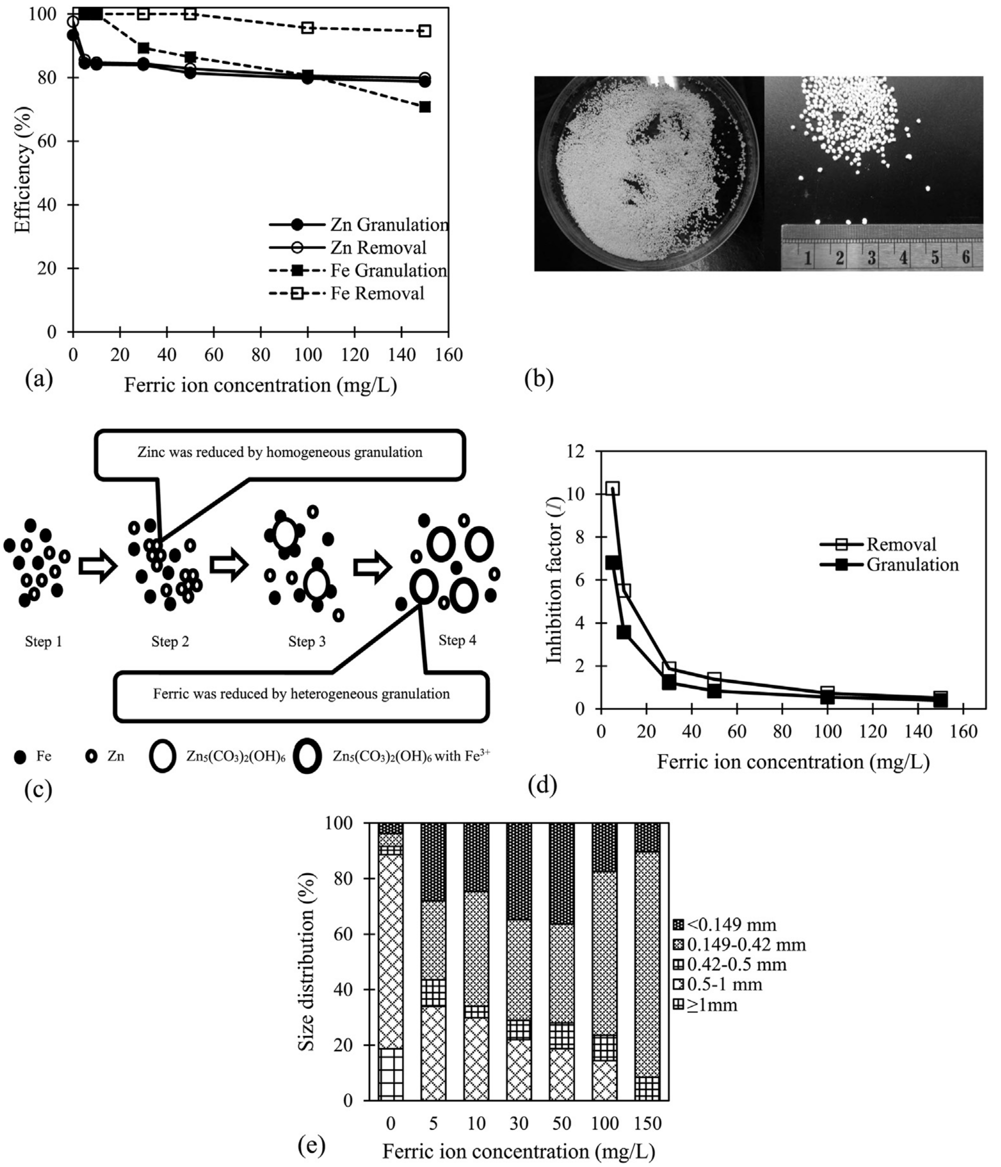

Fig. 6. (a) Effect of ferric ions on the removal and granulation efficiencies, (b) granules of hydrozincite products without ferric ions, and the ferric ion: (c) reaction mechanism, (d) inhibition factor on the removal and granulation efficiencies and (e) its granules size distribution.

In the absence of ferric ions, the Zn removal and granulation efficiencies were 97.56% and 93.39%. In contrast, in the presence of ferric ions, the efficiencies dropped from 12.27% to 18.17% (Zn removal) and from 9.49% to 15.68% (granulation). The percentage of Zn removal and granulation efficiencies were very close indicating that Zn precipitated mainly via homogeneous granulation process. Conversely, ferric ions were reduced by the heterogeneous granulation process as shown in the reaction mechanism in Fig. 6 (c). Ferric ions were completely removed at a concentration of 50 mg/L and below. Furthermore, the removal efficiencies based on the ferric ion loading reached 95.63% (100 mg/L) and 94.65% (150 mg/L). The respective granulation efficiencies reached 100% (5 mg/L), 100% (10 mg/L), 89.33% (30 mg/L), 86.48% (50 mg/L), 80.75% (100 mg/L) and 70.80% (150 mg/L). Since the amount of $Fe(OH)_3$ nuclei formed was minimal as compared to the presence of hydrozincite, the available active sites for crystallization on hydrozincite surface became dominant; hence, the crystallization of iron occurred via heterogeneous pathway (Anotai et al., 2018).

The inhibition of ferric ions on the Zn removal and granulation efficiencies can be defined in Eq. (12):

$$I = \frac{\Delta R_{Zn}}{\Delta C_{Fe}} \tag{12}$$

where I is the inhibition factor, ΔR_{Zn} (mg/L) refers to the difference of the Zn residual with and without ferric ions and ΔC_{Fe} (mg/L) pertains to the change of ferric ion concentration in the system.

From Fig. 6 (d), it can be seen that increasing the ferric ion concentration decreases the inhibition of ferric ions on the efficiencies towards Zn removal and granulation. As ferric ion concentration was increased from 5 mg/L to 150 mg/L, the inhibition of ferric ions decreased the efficiencies from 10.26% to 0.51% (Zn removal) and from 6.80% to 0.39% (granulation). The results indicated a limited amount of ferric ions can cause an inhibition on the granules that affects the efficiencies of Zn removal and granulation. The efficiencies at 5 mg/L Fe^{3+} specifically reached 85.59% (Zn removal) and 84.52% (granulation). When the ferric ion concentration was increased from 10 mg/L to 150 mg/L, Zn removal and granulation efficiencies dropped due to the occurring inhibition towards crystallization.

Moreover, the ferric ion concentration also affected the granulation size based on Fig. 6 (e). In the absence of ferric ions, the percentage of granule diameter with 1.0 mm and more was 18.71%. However, the granules with a diameter of 1.0 mm and more was non-existing in the presence of ferric ions (5 mg/L to 150 mg/L). All of the formed granules were having sizes below 0.5 mm. The resulting composition of granules with a diameter of 0.5 mm–1 mm were 34.02% (5 mg/L Fe^{3+}), 29.9% (10 mg/L Fe^{3+}), 21.93% (30 mg/L Fe^{3+}), 18.75% (50 mg/L Fe^{3+}), 14.42% (100 mg/L Fe^{3+}) and 0% (150 mg/L Fe^{3+}). This implies that ferric ions could essentially decrease the granule size significantly due to the interaction of Fe^{3+} and the presence of OH^- at the FBR. This evidently indicates that the presence of ferric ions is able to inhibit the granules of Zn.

3.9. Analysis of minimum fluid velocity

In order to effectively establish fluidization, the upflow stream is required to surpass the minimum fluid velocity (U_{mf}: cm/s) in which the gravitational force on the particles are maintained at a fluidized state (Chen et al., 2015). This hydrodynamic characteristic can be determined through the Ergun equation in Eq. (13) to appropriately identify the upflow of the bed that would instigate fluidization (Gupta et al., 2009; Sau et al., 2007).

$$U_{mf} = \frac{\varnothing^2 D^2 \varepsilon_{mf}^3 (\rho_S - \rho_W) G}{150\mu\left(1 - \varepsilon_{mf}\right)} \tag{13}$$

where $\varnothing$ refers to the sphericity, D denotes the average diameter (μm) of the fluidized particles, ρ_S and ρ_W are the densities of hydrozincite and water, G represents the gravitational acceleration (980 cm s^{-2}), μ signifies the viscosity of water and ε_{mf} indicates the voidage at the minimum fluidization.

The addition of 7,000 mg/L chloride content led to the crystal formation in the FBHG process with a nominal size of 149 μm (D), while the incorporation of 150 mg/L ferric ions resulted to crystal sizes of 42 μm (D). The simulated solution is constituted by a homogeneous hydrozincite ($\rho_S = 3.5$ g/cm^3) and water ($\rho_W = 1.0$ g/cm^3 and $\mu = 0.00894$ g/cm–s). The subsequent products take the form of a sharp sand like shaped crystals that has a $\varnothing$ of 0.67 (Geankoplis et al., 2018). The minimum fluidization is typically achieved at the ε_{mf} value of 0.5 (Inglezakis and Poulopoulos, 2006). As a result, the FBHG process showed that the U_{mf} upon independently mixing chloride and ferric ions are 16.4 cm/s and 4.1 cm/s. This implies that the experimental upflow times (0.4–1.9 cm/s) for the calculated minimum fluidized velocity of the solution with ferric ions are conducted more than that in the solution with chloride content.

4. Conclusions

In this study, the treatability and parameters that affect the efficiencies of Zn removal and granulation were investigated by identifying the mechanisms of the FBHG process that stimulates the production of granules. The results from this study can be summarized and concluded as follows: (1) Higher removal and granulation efficiencies were obtained in the FBHG than in the FBG process. (2) The most favorable operating parameters for hydrozincite granulation were at a [CO_3^{2-}]:[Zn^{2+}] molar ratio of 1.2 and pH 7.2. The removal efficiency lowered from 97.60% to 89.29%, while the granulation efficiency decreased from 92.49% to 86.67%. (3) At a granule diameter of 0.5 mm–1.0 mm, 70.0% and 45.3% of the total weight were formed in the absence and presence of chloride. (4) Ferric ion concentration can inhibit the formation of the granules and influence the efficiencies of Zn removal and granulation. Moreover, this can alter the color of the granules from white to orange, but the structure of the granules is unaffected. (5) The data of the characterized products by XRD, EDS and SEM confirmed by the results of hydrozincite. The morphology consisted botryoidal masses and Zn composition of 63.71 wt% (absence of electrolyte), 63.08 wt% (with chloride) and 52.62 wt% (with ferric ions). Furthermore, future research directions in-line with this study may include the following: (1) Process optimization using the response surface methodology to determine the optimum parameters for Zn removal. (2) The investigation of the combined effect of chloride and ferric ions in the hydrozincite formation. (3) A comprehensive kinetic analysis with respect to Zn removal in the FBHG process. (4) The utilization of real wastewater and a detailed analysis of its ion species.

Acknowledgments

The authors would like to acknowledge the Taiwan Ministry of Science and Technology (MOST 102-2221-E-041-001-MY3) and National Research Foundation of Korea through Ministry of Education (No. 2016R1A6A1A03012812) for the financial support of this research.

Appendix A. Supplementary data

Supplementary data to this article can be found online at https://doi.org/10.1016/j.jclepro.2019.05.192.

References

Anotai, J., Wasukran, N., Boonrattanakij, N., 2018. Heterogeneous fluidized-bed Fenton process: factors affecting iron removal and tertiary treatment application. Chem. Eng. J. 352, 247–254. https://doi.org/10.1016/j.cej.2018.07.037.

Babilas, D., Dydo, P., 2018. Selective zinc recovery from electroplating wastewaters by electrodialysis enhanced with complex formation. Separ. Purif. Technol. 192, 419–428. https://doi.org/10.1016/j.seppur.2017.10.013.

Ballesteros, F.C., Salcedo, A.F.S., Vilando, A.C., Huang, Y.H., Lu, M.C., 2016. Removal of nickel by homogeneous granulation in a fluidized-bed reactor. Chemosphere 164, 59–67. https://doi.org/10.1016/j.chemosphere.2016.08.081.

Benjamin, M.M., 2015. Water Chemistry, second ed. Waveland Press, Incorporated, Long Grove, IL.

Benjamin, M.M., 2001. Water Chemistry, first ed. McGraw-Hill Higher Education, Europe.

Bhattacharya, A.K., Mandal, S.N., Das, S.K., 2006. Adsorption of Zn(II) from aqueous solution by using different adsorbents. Chem. Eng. J. 123, 43–51. https://doi.org/10.1016/j.cej.2006.06.012.

Boonrattanakij, N., Sakul, W., Garcia-Segura, S., Lu, M.C., 2018. Implementation of fluidized-bed Fenton as pre-treatment to reduce chemical oxygen demand of wastewater from screw manufacture: influence of reagents feeding mode. Separ. Purif. Technol. 202, 275–280. https://doi.org/10.1016/j.seppur.2018.03.075.

Caddarao, P.S., Garcia-Segura, S., Ballesteros, F.C., Huang, Y.H., Lu, M.C., 2018. Phosphorous recovery by means of fluidized bed homogeneous crystallization of calcium phosphate. Influence of operational variables and electrolytes on brushite homogeneous crystallization. J. Taiwan Inst. Chem. Eng. 83, 124–132. https://doi.org/10.1016/j.jtice.2017.12.009.

Chen, C.S., Shih, Y.J., Huang, Y.H., 2015. Remediation of lead (Pb(II)) wastewater through recovery of lead carbonate in a fluidized-bed homogeneous crystallization (FBHC) system. Chem. Eng. J. 279, 120–128. https://doi.org/10.1016/j.cej.2015.05.013.

Cheng, J., Poduska, K., 2013. A strategy for hydroxide exclusion in nanocrystalline solid-state metathesis products. Nanomaterials 3, 317–324. https://doi.org/10.3390/nano3030317.

Chung, J., Jeong, E., Choi, J.W., Yun, S.T., Maeng, S.K., Hong, S.W., 2015. Factors affecting crystallization of copper sulfide in fed-batch fluidized bed reactor. Hydrometallurgy 152, 107–112. https://doi.org/10.1016/j.hydromet.2014.12.014.

Clever, H.L., Derrick, M.E., Johnson, S.A., 1992. The solubility of some sparingly soluble salts of zinc and cadmium in water and in aqueous electrolyte solutions. J. Phys. Chem. Ref. Data 21, 943–967. https://doi.org/10.1063/1.555909.

Connick, R.E., Hepler, L.G., Hugus, Z.Z., Kury, J.W., Latimer, W.M., Tsao, M.S., 1956. The complexing of Iron(III) by fluoride ions in aqueous solution: free energies, heats. J. Am. Chem. Soc. 78, 1827–1829. https://doi.org/10.1021/ja01590a015.

De Luna, M.D.G., Bellotindos, L.M., Asiao, R.N., Lu, M.C., 2015. Removal and recovery of lead in a fluidized-bed reactor by crystallization process. Hydrometallurgy 155, 6–12. https://doi.org/10.1016/j.hydromet.2015.03.009.

De Luna, M.D.G., Rance, D.P.M., Bellotindos, L.M., Lu, M.C., 2017. Removal of sulfate by fluidized bed crystallization process. J. Environ. Chem. Eng. 5, 2431–2439. https://doi.org/10.1016/j.jece.2017.04.052.

Fischer, R.B., Peters, D., 1970. Chemical Equilibrium, first ed. W.B. Saunders Company, Toronto, Canada.

Forslund, M., Leygraf, C., Claesson, P.M., Pan, J., 2014. Octadecanethiol as corrosion inhibitor for zinc and patterned zinc-copper in humidified air with formic acid. J. Electrochem. Soc. 161, C330–C338. https://doi.org/10.1149/2.089406jes.

Freitas, E.D. de, Almeida, H.J. de, Vieira, M.G.A., 2017. Binary adsorption of zinc and copper on expanded vermiculite using a fixed bed column. Appl. Clay Sci. 146, 503–509. https://doi.org/10.1016/j.clay.2017.07.004.

Geankoplis, C.J., Hersel, A.A., Lepek, D.H., 2018. Transport processes and separation process principles. In: Transport Processes and Separation Process Principles, fifth ed. Prentice Hall.

Guevara, H.P.R., Ballesteros, F.C., Vilando, A.C., de Luna, M.D.G., Lu, M.C., 2017. Recovery of oxalate from bauxite wastewater using fluidized-bed homogeneous granulation process. J. Clean. Prod. 154, 130–138. https://doi.org/10.1016/j.jclepro.2017.03.172.

Gupta, S.K., Agarwal, V.K., Singh, S.N., Seshadri, V., Mills, D., Singh, J., Prakash, C., 2009. Prediction of minimum fluidization velocity for fine tailings materials. Powder Technol. 196, 263–271. https://doi.org/10.1016/j.powtec.2009.08.003.

Inglezakis, V.J., Poulopoulos, S.G., 2006. Adsorption, ion exchange and catalysis: design of operations and environmental applications. In: Adsorption, Ion Exchange and Catalysis. Elsevier. https://doi.org/10.1016/B978-044452783-7/50005-7.

Järvinen, M.A., Paavola, M., Poutiainen, S., Itkonen, P., Pasanen, V., Uljas, K., Leiviskä, K., Juuti, M., Ketolainen, J., Järvinen, K., 2015. Comparison of a continuous ring layer wet granulation process with batch high shear and fluidized bed granulation processes. Powder Technol. 275, 113–120. https://doi.org/10.1016/j.powtec.2015.01.071.

Lee, C.H., Lee, C.H., 2005. A study on nickel hydroxide crystallization characteristics. Korean J. Chem. Eng. 22, 712–716. https://doi.org/10.1007/BF02705787.

Lei, C., Yan, B., Chen, T., Xiao, X.M., 2018. Preparation and adsorption characteristics for heavy metals of active silicon adsorbent from leaching residue of lead-zinc tailings. Environ. Sci. Pollut. Res. 25, 21233–21242. https://doi.org/10.1007/s11356-018-2194-9.

Ngwenya, B.T., Magennis, M., Podda, F., Gromov, A., 2014. Self-preservation strategies during bacterial biomineralization with reference to hydrozincite and implications for fossilization of bacteria. J. R. Soc. Interface 11. https://doi.org/10.1098/rsif.2014.0845.

Peng, C., Jin, R., Li, G., Li, F., Gu, Q., 2014. Recovery of nickel and water from wastewater with electrochemical combination process. Sep. Purif. Technol. 136, 42–49. https://doi.org/10.1016/j.seppur.2014.08.025.

Porea, T.J., Belmont, J.W., Maboney, D.H., 2000. Zinc-induced anemia and neutropenia in an adolescent. J. Pediatr. 136, 688–690. https://doi.org/10.1067/mpd.2000.103355.

Quiton, K.G., Doma, B., Futalan, C.M., Wan, M.W., 2018. Removal of chromium(VI) and zinc(II) from aqueous solution using kaolin-supported bacterial biofilms of Gram-negative E. coli and Gram-positive Staphylococcus epidermidis. Sustain. Environ. Res. 28, 206–213. https://doi.org/10.1016/j.serj.2018.04.002.

Rahaman, M.S., Mavinic, D.S., 2009. Recovering nutrients from wastewater treatment plants through struvite crystallization: CFD modelling of the hydrodynamics of UBC MAP fluidized-bed crystallizer. Water Sci. Technol. 59, 1887–1892. https://doi.org/10.2166/wst.2009.214.

Salcedo, A.F.M., Ballesteros, F.C., Vilando, A.C., Lu, M.C., 2016. Nickel recovery from synthetic Watts bath electroplating wastewater by homogeneous fluidized bed granulation process. Separ. Purif. Technol. 169, 128–136. https://doi.org/10.1016/j.seppur.2016.06.010.

Sau, D.C., Mohanty, S., Biswal, K.C., 2007. Minimum fluidization velocities and maximum bed pressure drops for gas-solid tapered fluidized beds. Chem. Eng. J. 132, 151–157. https://doi.org/10.1016/j.cej.2007.01.036.

Sethurajan, M., Lens, P.N.L., Rene, E.R., van de Vossenberg, J., Huguenot, D., Horn, H.A., Figueiredo, L.H.A., van Hullebusch, E.D., 2017. Bioleaching and selective biorecovery of zinc from zinc metallurgical leach residues from the Três Marias zinc plant (Minas Gerais, Brazil). J. Chem. Technol. Biotechnol. 92, 512–521. https://doi.org/10.1002/jctb.5026.

Shih, Y.J., Abarca, R.R.M., de Luna, M.D.G., Huang, Y.H., Lu, M.C., 2017. Recovery of phosphorus from synthetic wastewaters by struvite crystallization in a fluidized-bed reactor: effects of pH, phosphate concentration and coexisting ions. Chemosphere 173, 466–473. https://doi.org/10.1016/j.chemosphere.2017.01.088.

Su, C.C., Abarca, R.R.M., de Luna, M.D.G., Lu, M.C., 2014. Phosphate recovery from fluidized-bed wastewater by struvite crystallization technology. J. Taiwan Inst. Chem. Eng. 45, 2395–2402. https://doi.org/10.1016/j.jtice.2014.04.002.

Tsai, W.C., Ibarra-Buscano, S., Kan, C.C., Futalan, C.M., Dalida, M.L.P., Wan, M.W., 2016. Removal of copper, nickel, lead, and zinc using chitosan-coated montmorillonite beads in single- and multi-metal system. Desalin. Water Treat. 57, 9799–9812. https://doi.org/10.1080/19443994.2015.1035676.

Vilando, A.C., Caparanga, A.R., Lu, M.-C., 2019. Enhanced recovery of aluminum from wastewater using a fluidized bed homogeneously dispersed granular reactor. Chemosphere 223, 330–341. https://doi.org/10.1016/j.chemosphere.2019.02.086.

Wang, Z., Gao, J., Shi, A., Meng, L., Guo, Z., 2018. Recovery of zinc from galvanizing dross by a method of super-gravity separation. J. Alloy. Comp. 735, 1997–2006. https://doi.org/10.1016/j.jallcom.2017.11.385.

WHO, 2003. Zinc in Drinking-Water. Background Document for Preparation of WHO Guidelines for Drinking-Water Quality. World Health Organization, Geneva.

Zheng, X., Li, J., Ma, A., Peng, J., Zhang, L., Yin, S., 2015. Zinc recovery from zinc oxide flue dust during the neutral leaching process by ultrasound. In: Carpenter, J.S., Bai, C., Escobedo, J.P., Hwang, J.-Y., Ikhmayies, S., Li, B., Li, J., Monteiro, S.N., Peng, Z., Zhang, M. (Eds.), Characterization of Minerals, Metals, and Materials 2015. Springer, Cham, pp. 563–570. https://doi.org/10.1007/978-3-319-48191-3_70.

Zhou, P., Huang, J.-C., Li, A.W.F., Wei, S., 1999. Heavy metal removal from wastewater in fluidized bed reactor. Water Res. 33, 1918–1924. https://doi.org/10.1016/S0043-1354(98)00376-5.